

FIGURE 9.1 Calculating the solid angle of a circular face.

over ϕ to get

$$d\Omega = 2\pi \sin \theta \, d\theta$$

and integrate from $\theta = 0$ to $\theta_{\max} = \tan^{-1}(R/d)$ to get

$$\frac{\Delta\Omega}{4\pi} = \frac{1}{2} \int_{\theta=0}^{\theta_{\max}} \sin \theta \, d\theta,$$

where we have written the fraction of the total solid angle as $\Delta\Omega/4\pi$. This integral is done most easily by a change of variables to $\mu = \cos \theta$ with μ ranging from $\cos \theta_{\max} = d/\sqrt{d^2 + R^2}$ to 1. Since $d\mu = -\sin \theta \, d\theta$,

$$\frac{\Delta\Omega}{4\pi} = \int_{\cos \theta_{\max}}^1 d\mu = \frac{1}{2} \left[1 - \frac{d}{(d^2 + R^2)^{1/2}} \right]. \quad (9.3)$$

For $d = 0$, $\Delta\Omega/4\pi = 1/2$, that is, the surface covers one entire hemisphere. For $d \rightarrow \infty$, expand Eq. (9.3) to first order in R/d to find $\Delta\Omega/4\pi = R^2/4d^2$ or $\Delta\Omega = (\pi R^2)/d^2$, which is just what you expect from the basic definition of solid angle.

9.2. COMPTON SCATTERING

9.2.1. Frequency Shift and Cross Section

This section deals with the scattering of electromagnetic radiation by free electrons. As mentioned in the introduction to this chapter, it is the scattering of electromagnetic radiation from various objects that makes it possible for us to “see” them. However, as the frequency of the radiation is increased beyond the visible region, the light quanta have energies comparable to, or larger than, the binding energy of the electrons in atoms, and the electrons can therefore be considered as free.

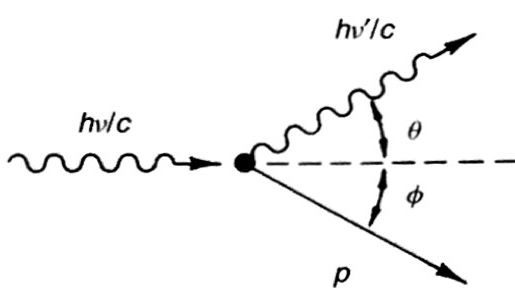


FIGURE 9.2 Compton scattering of a photon from a free electron.

In 1920 A. H. Compton investigated the scattering of monochromatic X-rays from various materials. He observed that after the scattering, the energy (frequency) of the X-rays had changed, and had always decreased. From the point of view of classical electromagnetic theory, this frequency shift cannot be explained,¹ since the frequency is a property of the incoming electromagnetic wave (field) and cannot be altered by the change of direction implied by the scattering. If, on the other hand, we think of the incoming radiation as being represented by a beam of photons, we need only consider the scattering of a quantum of energy $E = h\nu$ from a free electron; then, because of energy-momentum conservation, the scattered quantum has energy $E' = h\nu' < E$, in complete agreement with the experiments of Compton.

The frequency shift will depend on the angle of scattering and can be easily calculated from the kinematics. Consider an incoming photon of energy $E = h\nu$ and momentum $h\nu/c$ (Fig. 9.2) scattering from an electron (at rest) of mass m ; p is the momentum of the electron after scattering, and $h\nu'$ and $h\nu'/c$ are the energy and momentum of the photon after the scattering. The three vectors $h\nu/c$, $h\nu'/c$, p must lie on the same plane, and energy conservation yields

$$h\nu + mc^2 = h\nu' + \sqrt{p^2 c^2 + m^2 c^4}. \quad (9.4)$$

From momentum conservation we obtain

$$h\nu = h\nu' \cos \theta + cp \cos \phi \quad (9.5)$$

$$0 = h\nu' \sin \theta - cp \sin \phi. \quad (9.6)$$

¹See, for example, J. D. Jackson, *Classical Electrodynamics*, 3rd ed., p. 694, Wiley, New York, 1999.

Here θ is the photon scattering angle, and ϕ the electron recoil angle. To solve the above equations we transpose appropriately, square, and add Eq. (9.5) and Eq. (9.6) to obtain

$$h^2\nu^2 - 2h^2\nu\nu'\cos\theta + h^2\nu'^2 = c^2p^2.$$

By squaring Eq. (9.4) we obtain

$$h^2\nu^2 + h^2\nu'^2 - 2h^2\nu\nu' + 2hmc^2(\nu - \nu') = c^2p^2,$$

and subtraction of the two above expressions yields

$$\frac{\nu - \nu'}{\nu\nu'} = \frac{h}{mc^2}(1 - \cos\theta). \quad (9.7)$$

We can recast Eq. (9.7) into two more familiar forms: (a) to give the shift in wavelength of the scattered X-ray beam

$$\Delta\lambda = \lambda' - \lambda = \frac{h}{mc}(1 - \cos\theta) \quad (9.8)$$

or (b) to give the energy of the scattered photon

$$E' = \frac{E}{1 + (E/mc^2)(1 - \cos\theta)}. \quad (9.9)$$

From Eq. (9.8) we see that the shift in wavelength, except for the angular dependence, is a constant, the Compton wavelength²

$$h/mc = 2.42 \times 10^{-10} \text{ cm} = 0.0242 \text{ \AA}.$$

For low-energy photons, with $\lambda \gg 0.02 \text{ \AA}$, the Compton shift is very small, whereas for high-energy photons with $\lambda \ll 0.02 \text{ \AA}$, the wavelength of the *scattered* radiation is always on the order of 0.02 \AA , the Compton wavelength. These conclusions can equally well be obtained from Eq. (9.9), where the energy shift increases when E/mc^2 becomes large. For $E/mc^2 \gg 1$, E' is independent of E and on the order of $E' \approx mc^2$. Hence $\lambda' = c/\nu' = c/(E'/h) \sim c/(mc^2/h) = h/mc$ as stated before.

As an example, in this laboratory gamma rays from ^{137}Cs are scattered from an aluminum target; since $E = 0.662 \text{ MeV}$, we have $E/mc^2 = 1.29$, so that backscattered gamma rays ($\theta = 180^\circ$) will have $E' = E/3.6$,

²The mass of the electron m_e was used in evaluating h/mc ; by using the mass of the pion, or another particle, we obtain the pion Compton wavelength, and so forth.

which is less than 30% of their original energy. It thus becomes quite easy to observe the Compton energy shift as compared to X-ray scattering, where, if we assume $\lambda = 2 \text{ \AA}$, $\Delta\lambda/\lambda = \Delta E/E = 0.01$.

In the original experiments Compton and his collaborators observed (especially for high Z materials) in addition to the frequency-shifted X-rays, scattered radiation *not shifted* in frequency. The unshifted X-rays are due to scattering from electrons that remained bound in the atom³: in this process the recoiling system is the entire atom, and we replace in Eq. (9.8) m by m_A (where $m_A \approx 2000 \times A \times m_e$), resulting in an undetectable wavelength shift, $\Delta\lambda' \approx 10^{-7} \text{ \AA}$.

Next we are interested in the differential cross section for the scattering of the radiation from the electrons. Classically this is given by the Thomson cross section,⁴ which can be easily derived: consider a plane wave propagating in the z direction with the \mathbf{E} vector linearly polarized along the x direction. This is incident on an electron of mass m , as shown in Fig. 9.3. The electron will experience a force $F = eE = eE_0 \cos \omega t$, and its acceleration will be

$$\ddot{v} = \frac{eE_0}{m} \cos \omega t.$$

According to Eq. (8.27), the power radiated by this accelerated electron will be (nonrelativistically, in SI units)

$$\frac{dP}{d\Omega} = \frac{1}{4\pi} \frac{e^2}{4\pi\epsilon_0} \frac{1}{c^3} \dot{v}^2 \sin^2 \Theta, \quad (9.10)$$

where Θ is the angle between the direction of observation and the \mathbf{E} vector of the incoming wave. Using the expression for \dot{v} , we can write for Eq. (9.10) averaged over one cycle

$$\left\langle \frac{dP}{d\Omega} \right\rangle = \frac{1}{2} \left(\frac{e^2}{4\pi\epsilon_0 mc^2} \right)^2 \epsilon_0 E_0^2 c \sin^2 \Theta.$$

Finally, from the definition of the cross section (see Section 8.2.1.a) we have

$$\frac{d\sigma}{d\Omega} = \frac{\text{energy radiated/(unit time - unit solid angle)}}{\text{incident energy/(unit area - unit time)}}.$$

³A similar situation is discussed in the following section on the Mössbauer effect, where the nucleus remains bound in the lattice and the recoiling system is the entire crystal.

⁴See also Section 8.2.5.

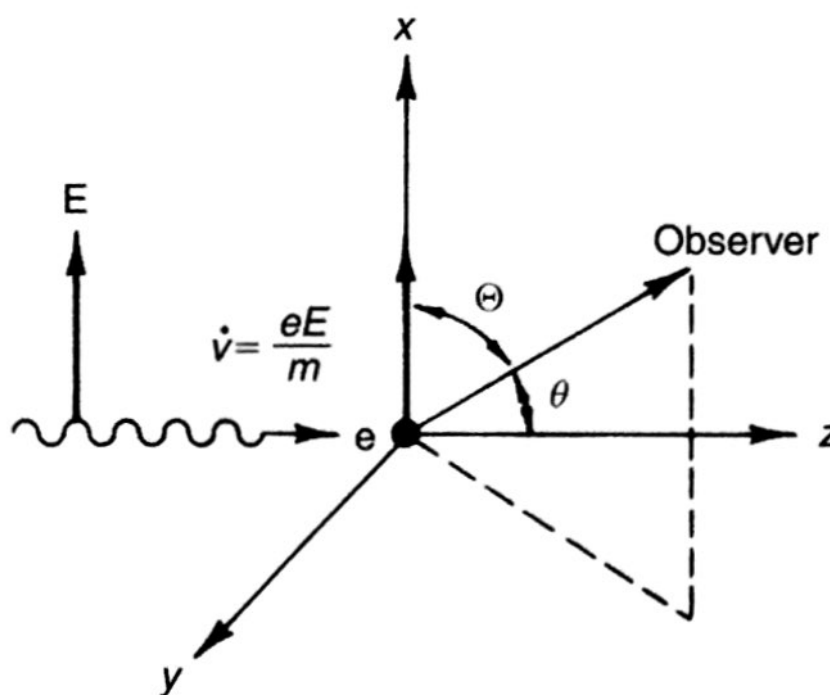


FIGURE 9.3 Classical picture of the scattering of electromagnetic radiation by an electron; this leads to the Thomson cross section.

Here the denominator is clearly given by the Poynting vector

$$\langle I \rangle = \frac{1}{2} \sqrt{\frac{\epsilon_0}{\mu_0}} E_0^2 = \frac{1}{2} \epsilon_0 c E_0^2.$$

Thus we obtain

$$\frac{d\sigma}{d\Omega} = \left(\frac{e^2}{4\pi\epsilon_0 mc^2} \right)^2 \sin^2 \Theta, \quad (9.11)$$

where

$$\frac{e^2}{4\pi\epsilon_0 mc^2} = r_0$$

has dimensions of length, and is referred to as the “classical electron radius”

$$r_0 = 2.82 \times 10^{-13} \text{ cm.}$$

Finally, we average over all possible directions of polarization of the incoming wave and use the angle θ measured from the direction of propagation of the incident wave to obtain

$$\frac{d\sigma}{d\Omega} = r_0^2 \left(\frac{1 + \cos^2 \theta}{2} \right). \quad (9.12)$$

When integrated over all angles, Eq. (9.12) yields the Thomson cross section

$$\sigma_T = \frac{8\pi}{3} r_0^2. \quad (9.13)$$

(This result was given without proof in Eq. (8.21).)

Several objections can be raised to the simple cross section given by Eq. (9.12) or Eq. (9.13): (a) it does not depend on frequency, a fact not supported by experiment; (b) the electron, even though free, is assumed not to recoil; (c) the treatment is nonrelativistic; and (d) quantum effects are not taken into account. Indeed, the correct quantum-mechanical calculation for Compton scattering yields the so called Klein–Nishina formula⁵

$$\begin{aligned} \frac{d\sigma}{d\Omega} = r_0^2 \frac{1 + \cos^2 \theta}{2} & \frac{1}{[1 + \gamma(1 - \cos \theta)]^2} \\ & \times \left[1 + \frac{\gamma^2(1 - \cos \theta)^2}{(1 + \cos^2 \theta)[1 + \gamma(1 - \cos \theta)]} \right], \end{aligned} \quad (9.14)$$

where r_0 and θ were defined previously, and $\gamma = h\nu/mc^2$. The cross section has been averaged over incoming (and summed over outgoing) polarizations. By integrating Eq. (9.14), the total cross section can be obtained. We will not give the complete result here, but the asymptotic expressions have already been presented in Eq. (8.22).

A comparison of the Thomson (Eq. (9.12)) and Klein–Nishina cross sections, including the results obtained in this laboratory for $\gamma = 1.29$, is shown in Fig. 9.8. We remark that although the Thomson cross section is symmetric about 90° , the Klein–Nishina cross section is peaked forward strongly as γ increases. This is due to a great extent to kinematical factors associated with the Lorentz transformation from the center of mass to the laboratory; note that the center-of-mass velocity of the (incident gamma ray + free electron) system is

$$\bar{v} = c\bar{\beta} = c\gamma/(1 + \gamma),$$

where as before $\gamma = h\nu/mc^2$.

The experimental data are in perfect agreement with the results of Eqs. (9.9) and (9.14), which are among the most impressive and convincing

⁵See for instance F. Gross, *Relativistic Quantum Mechanics and Field Theory*, Section 10.5, Wiley, New York, 1993.

successes of quantum theory. In the following two sections we will describe the experimental verification of these predictions.

9.2.2. The Compton Scattering Experiment

As with any scattering experiment, the apparatus will consist of:

- (a) The beam of incident particles, in this case photons,
- (b) The target (containing the electrons from which the photons scatter), and
- (c) The detector of the scattered photons.

The beam of photons is obtained by collimating the gamma radiation from a ^{137}Cs source. An intense source is required in order to get an appreciable counting rate for the scattered photons. As shown in Fig. 8.21 ^{137}Cs (^{137}Ba) emits a gamma ray of energy 0.662 MeV, and the detection techniques have been discussed in Chapter 8. Figure 8.21 also shows the pulse-height spectrum of the gamma radiation from ^{137}Cs , as obtained with standard equipment; the same detection equipment is used in this experiment with the only difference that heavy shielding is needed to prevent the detector from seeing the intense ^{137}Cs source directly.

A schematic of the apparatus is shown in Fig. 9.4. The lead pig *A* is fixed and holds the source, which can be introduced through the vertical hole (*V*). Another lead shield *B* contains the detector and can be rotated about the center, where the target is located. The lead assemblies are rather heavy (approximately 100 lb) and some provisions must be taken for adequate mounting.

For the source, a 7-mCi ^{137}Cs sample was used, which was properly encapsulated before being shipped to the laboratory. It should always be transported in a lead container, and when transferred into the lead pig *A*, it must be handled only by the attached string. The source holder (*A*) has a collimator (*h*) drilled horizontally, subtending a solid angle on the order of 0.03 sr. Of interest to us will be the density of the photon beam at the target, and the *expected* value is

$$\frac{3.7 \times 10^{10} \times 0.007}{4\pi} \frac{1}{r^2} = 1.3 \times 10^4 \text{ photons/cm}^2\text{-s},$$

where we use a source-to-detector distance $r = 40$ cm, for the data presented here.

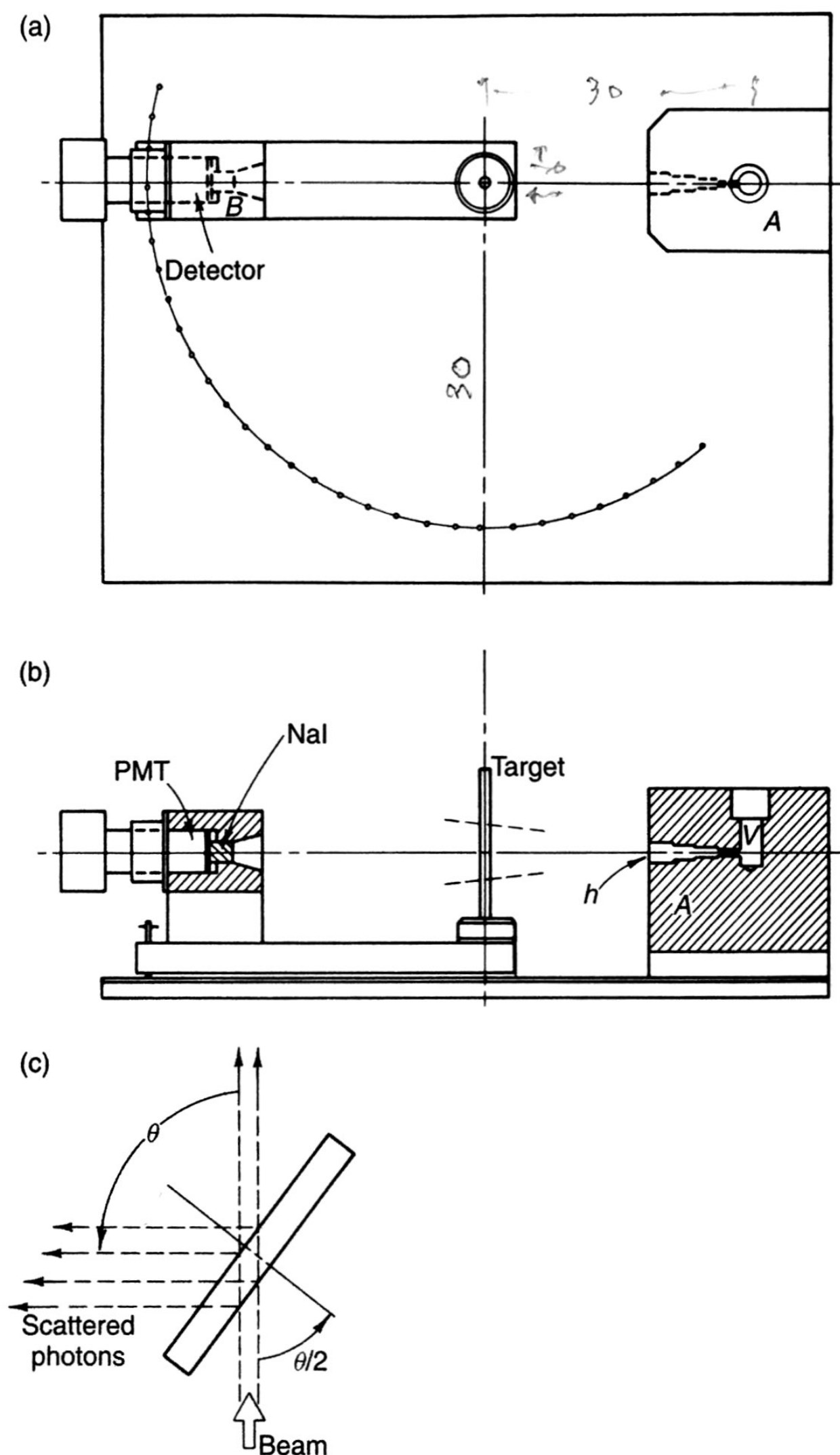


FIGURE 9.4 Schematic of an apparatus that can be used for measuring the Compton scattering of ^{137}Cs gamma rays from different targets: (a) top view and (b) elevation. The detector can be rotated relative to the beam direction, through a large angular range. Note that a less heavily shielded detector assembly is possible, but care needs to be taken so that the ^{137}Cs source is not directly visible to the detector at forward angles. (c) Use of a flat target when measuring Compton scattering at large angles. By such placement the scattered photons do not have to traverse very large amounts of the target material.

In contrast to the scattering of alpha particles, there is no need to enclose the beam and detector in vacuum or to use a very thin target. We know that gamma rays do not gradually lose energy when traversing matter as a charged particle does, but their interaction can be characterized by a mean free path. For the ^{137}Cs gamma ray we find that

$$\lambda = 4.7 \text{ cm in Al}, \quad \lambda = 0.92 \text{ cm in Pb};$$

this corresponds to 10^4 cm of air, so that the interaction of the photon beam in the air of the apparatus (approximately 100 cm) is indeed negligible. Also, the target thickness can safely be a fraction of a mean free path before the probability for multiple interactions becomes considerable. Aluminum targets $\frac{1}{2}$ in. thick are quite adequate for this experiment.

Some special mention must be made of the geometrical shape of the target. We may use a flat target (such as an aluminum plate), in which event the cross section is obtained by considering the interaction of the total beam with the number of electrons per square centimeter of the target⁶; alternatively, we may use a target of circular cross section (such as a rod), in which event the cross section is obtained by considering the interaction of the beam density (photons per square centimeter) with the total number of electrons in the target.⁷ When using a plate, it is advisable to rotate it so that it always bisects the angle between beam and detector, since otherwise the scattered photons may have to traverse a very large amount of material before leaving the target (see Fig. 9.4c). In that case, however, the amount of scattering material in the beam path varies as $1/\cos(\theta/2)$, and this correction must be applied to the yield of scattered particles. These effects are obviously eliminated when a target of circular cross section is used. In addition, the scattering point is better defined even if the beam is only poorly collimated. On the other hand, accurate evaluation of the flux density at the target is difficult. The results presented here were obtained by using a $\frac{3}{4}$ in.-diameter aluminum rod as the target.

An interesting refinement of the technique is made by observing the recoil electrons in time coincidence with the scattered photon. However, the kinetic energy of the recoil electron is

$$T_e = E - E' = E \frac{\gamma(1 - \cos\theta')}{1 + \gamma(1 - \cos\theta)},$$

⁶See Fig. 8.1.

⁷See Fig. 8.1.

which at its maximum value ($\theta = 180^\circ$) is

$$T(\text{electron}) = 0.662 \times (2.58/3.58) = 475 \text{ keV}.$$

The range of such an electron in aluminum is only 150 mg/cm^2 (see, for example, Feather's rule, Chapter 8, Eq. (8.15)), which corresponds to approximately 0.06 cm. Thus, the recoil electrons will, in almost all cases, stop in the target. On the other hand, if a plastic scintillator is used as the target, and is viewed with a photomultiplier, the recoil electrons do produce a signal that can be easily detected.

As mentioned before, the detection system consisted of a commercial NaI detector. The dimensions of the crystal were 3 in. diameter and 3 in. thick. Data was acquired with a multichannel analyzer, with a GPIB interface to a laptop computer. Figure 9.5 shows typical pulse-height spectra, taken at two different scattering angles (30° and 100°), and with the aluminum target rod both in and out of the beam, but with all running conditions otherwise identical. Each spectrum was acquired for 120 s. The difference between the target in and out spectra is also plotted.

By measuring the pulse-height distribution at various angles, we obtain the energy of the scattered photons as it is given by the position of the photopeak. This is most easily done by a simple Gaussian peak-fitting program to the photopeak as observed in the "background subtracted" spectra, for example, in the lower plots of Fig. 9.5. A rudimentary, but quite sufficient, Gaussian peak fit can be done in MATLAB by taking the logarithm of the net counts in the region of the photopeak, and fitting these to a second-order polynomial. To obtain the yield of scattered photons, we integrate the counts in the photopeak only and apply a correction for the "photofraction" or "peak-to-total ratio" as well as for crystal efficiency. These corrections depend on the crystal size and on the photon energy (which varies with angle). Figure 9.6 gives the peak-to-total ratio (for detectors at a specific distance from the photon source) and the detector efficiency, as a function of energy for several different NaI crystal dimensions.⁸

9.2.3. Results and Discussion

The results presented below were obtained by students using the apparatus described in the previous section.

⁸From *Efficiency Calculations for Selected Scintillators*, Bicron Corporation, available from the online library at <http://www.bicron.com>.

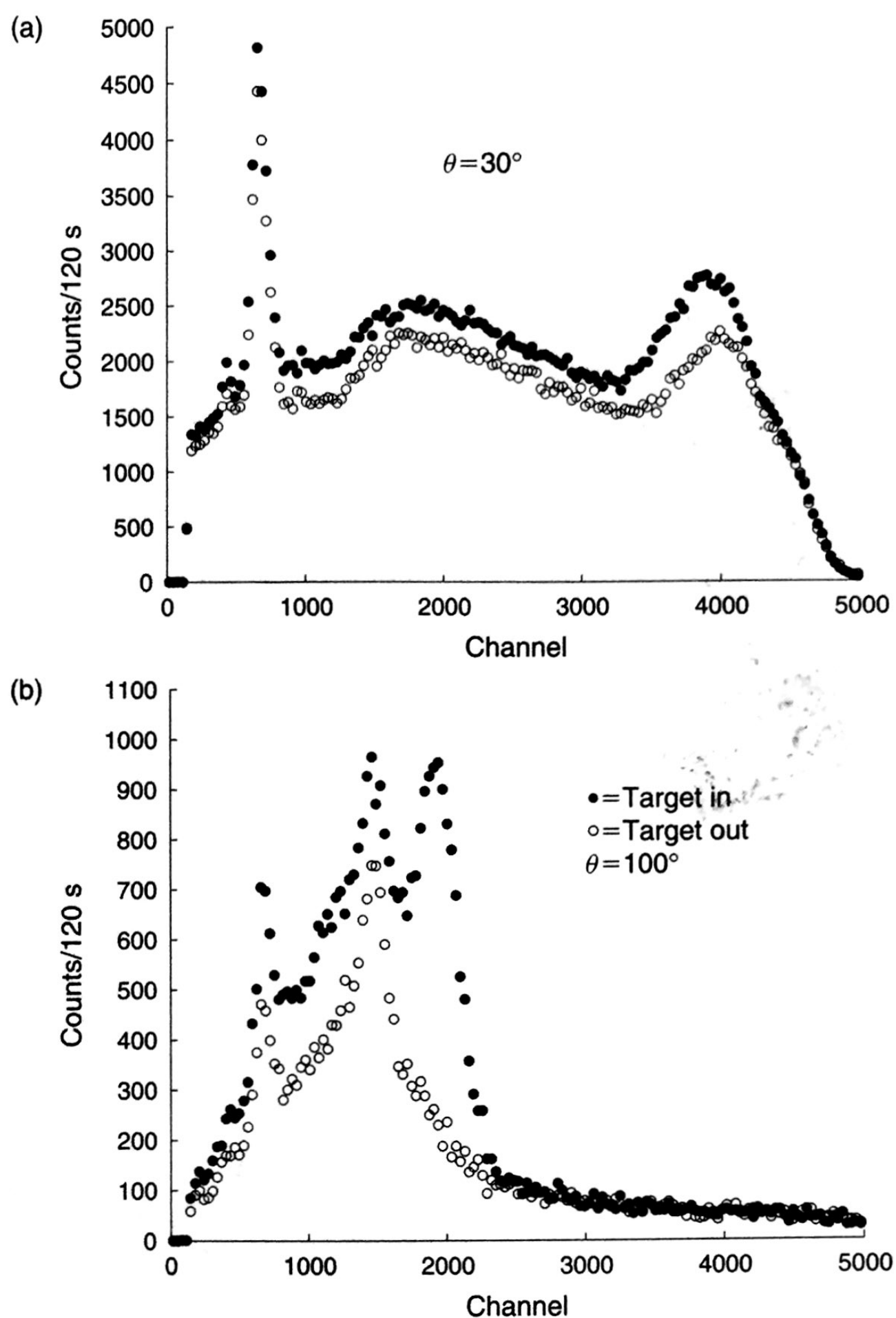
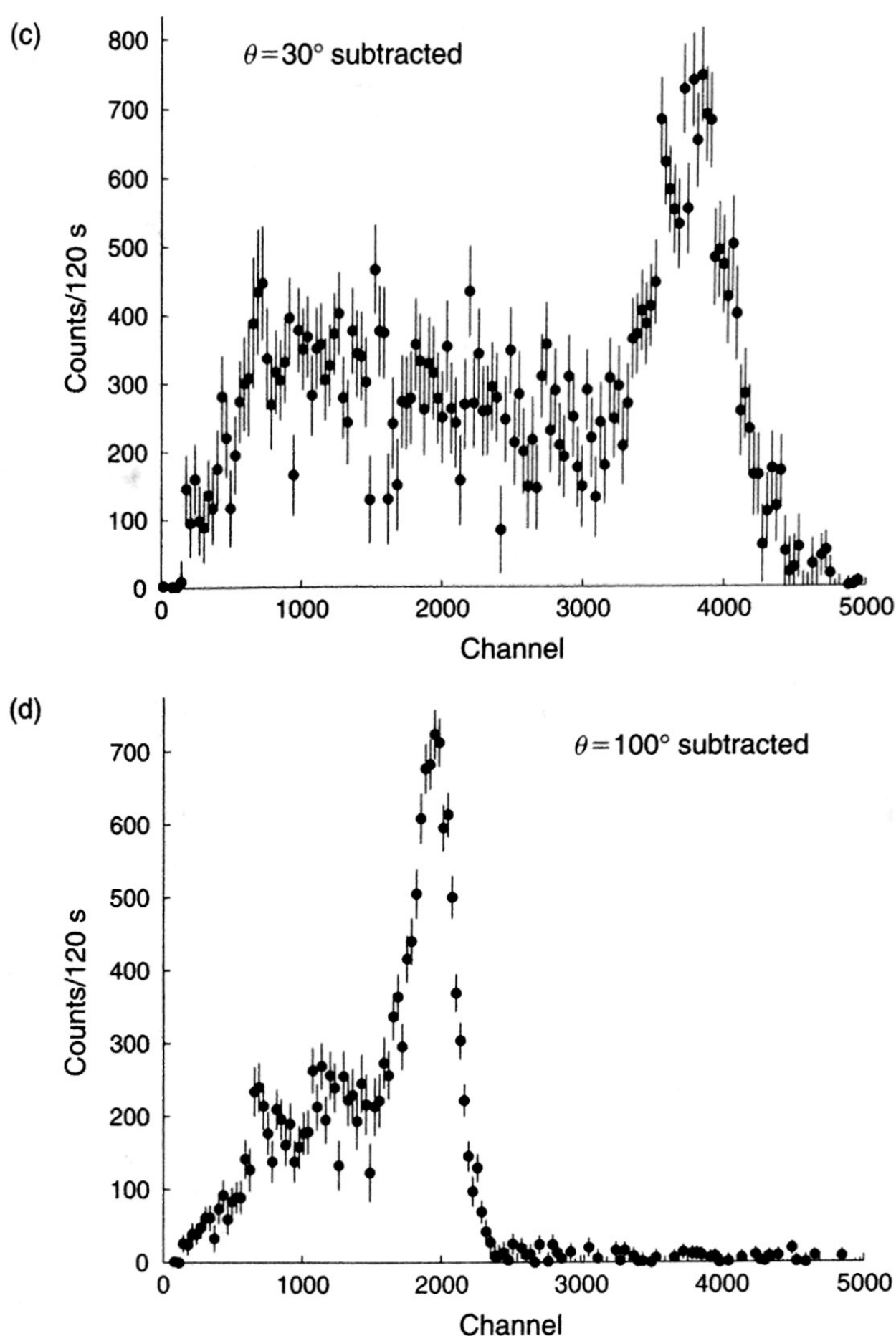


FIGURE 9.5 Pulse-height spectrum gamma rays in the Compton scattering apparatus. The plots (a), (b) show data acquired for 120 s both with the target rod in (solid points) and out (open circles) of the beam. At $\theta = 30^\circ$, the detector intercepts some fraction of the primary beam, and the rate is considerably larger than at $\theta = 100^\circ$. In addition, there are large signals due to K -shell X-rays and Compton backscattering in the lead shielding at both scattering angles. However, in each case, these background signals subtract cleanly away, leaving a pure Compton scattering signal from the aluminum target. The subtracted plots are shown in (c) and (d).

FIGURE 9.5 *Continued*

Before beginning measurements of Compton scattering, it is worthwhile to measure the beam profile of the ^{137}Cs source. This is best done by collimating the detector and putting it at a large distance from the source, so as to keep the count rate relatively low. (A number of difficulties arise at a high count rate, including severe dead time corrections and gain shifts, but these are negligible if the total rate is less than several kilohertz.) Then by moving the detector through different angles, one can map out the “shape” of the

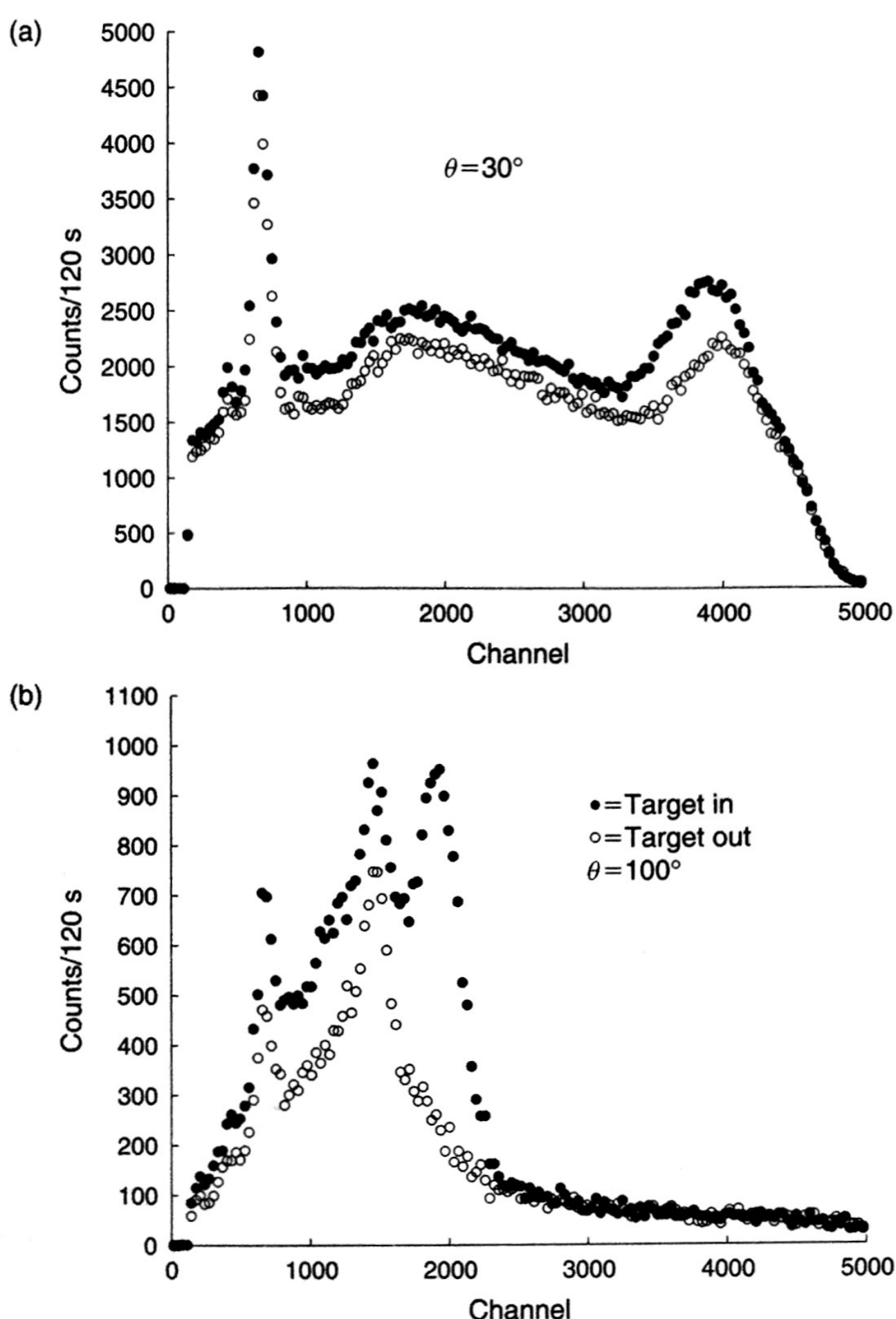
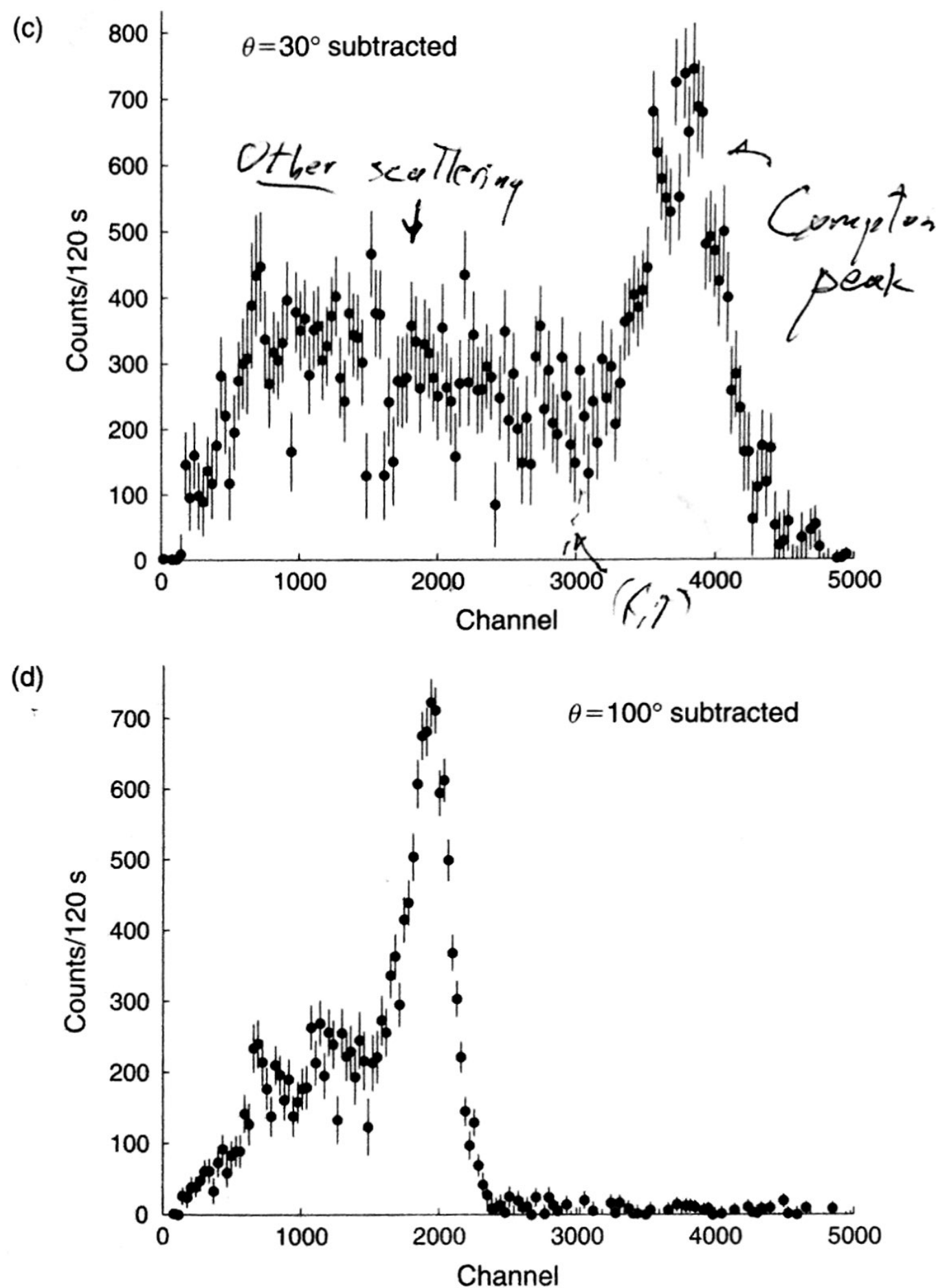


FIGURE 9.5 Pulse-height spectrum gamma rays in the Compton scattering apparatus. The plots (a), (b) show data acquired for 120 s both with the target rod in (solid points) and out (open circles) of the beam. At $\theta = 30^\circ$, the detector intercepts some fraction of the primary beam, and the rate is considerably larger than at $\theta = 100^\circ$. In addition, there are large signals due to K -shell X-rays and Compton backscattering in the lead shielding at both scattering angles. However, in each case, these background signals subtract cleanly away, leaving a pure Compton scattering signal from the aluminum target. The subtracted plots are shown in (c) and (d).

FIGURE 9.5 *Continued*

Before beginning measurements of Compton scattering, it is worthwhile to measure the beam profile of the ^{137}Cs source. This is best done by collimating the detector and putting it at a large distance from the source, so as to keep the count rate relatively low. (A number of difficulties arise at a high count rate, including severe dead time corrections and gain shifts, but these are negligible if the total rate is less than several kilohertz.) Then by moving the detector through different angles, one can map out the “shape” of the

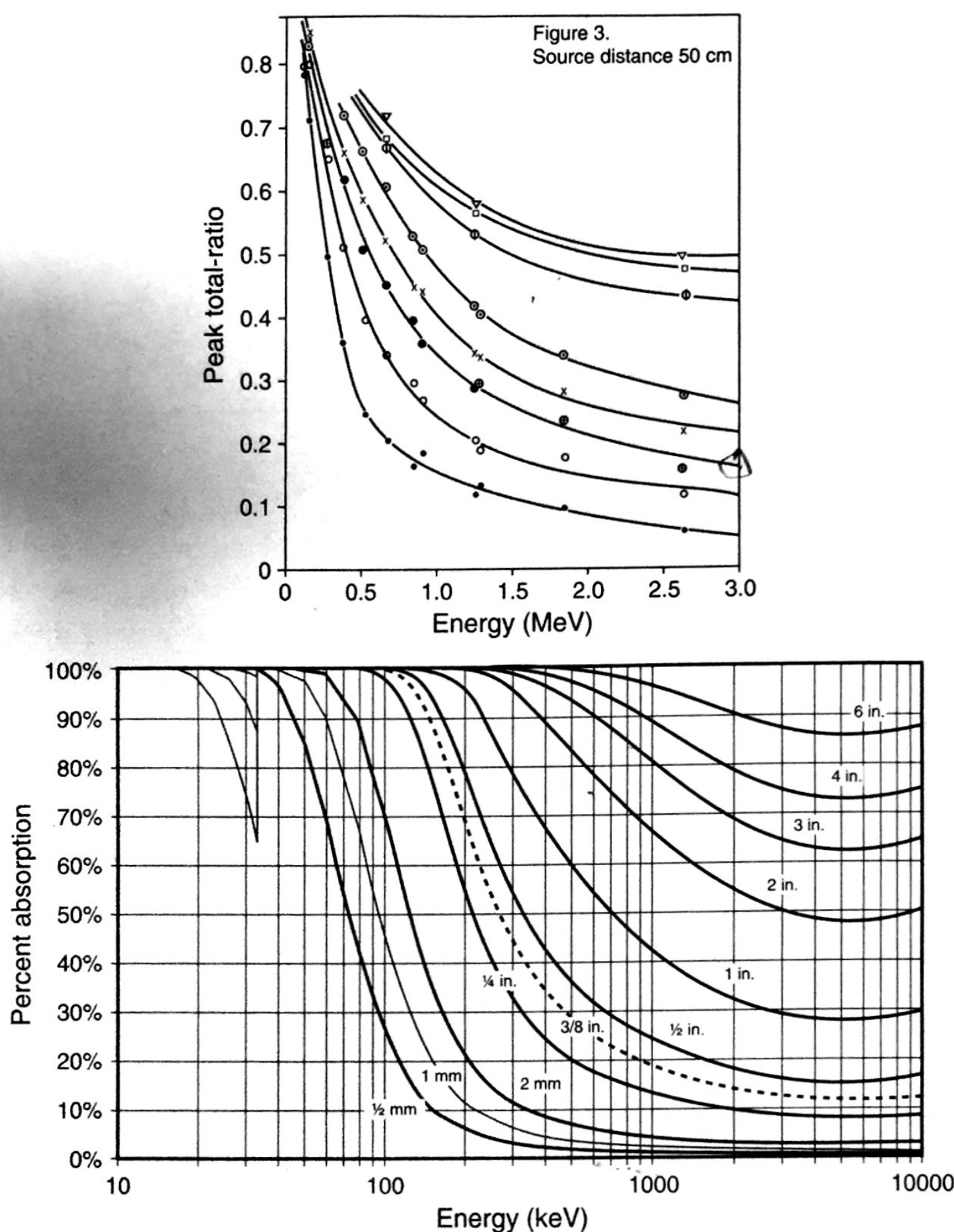


FIGURE 9.6 Detection efficiency plots for NaI crystals of various dimensions, from <http://www.bicron.com>. Shown are the peak-to-total ratio and the intrinsic absorption efficiency, all as a function of energy for various crystal dimensions.

photon beam. For our measurements here, however, we will simply assume the calculated beam flux for a measurement of the differential cross section.

Compton scattering data are taken by accumulating pulse-height spectra at various angles, both with the target in and out, for fixed periods of times. *In order to minimize the effects of gain drifts, and other changes over longer times, it is best to take the “in” and “out” spectra immediately*

TABLE 9.1 Summary of Compton Scattering Data

Angle (°)	Peak channel	Counts (in)	Counts (out)	E' (MeV)	Peak/total ratio	Efficiency	$d\sigma/d\Omega$ (10^{-27} cm 2 /sr)
20	4300	528,161	508,714	0.614	0.47	0.865	55.2
30	3732	97,663	81,121	0.564	0.50	0.890	42.9
40	3384	29,856	14,566	0.508	0.53	0.930	35.8
60	2810	16,382	5062	0.402	0.57	0.960	23.9
80	2258	16,268	6251	0.320	0.65	0.990	18.0
100	1922	17,482	7632	0.263	0.72	0.999	15.8

Note. Each spectrum was acquired for 120 s.

one after the other. (For example, see Fig. 9.5.) Data taken by students are summarized in Table 9.1. In this table, E' is the photon energy as calculated from Eq. (9.9), and is used to look up the peak-to-total ratio and the intrinsic efficiency from Fig. 9.6.

Radioactive sources are used to calibrate the analyzer channel in terms of photon energy. (See Fig. 8.24 and the associated text. It is advisable to carry out a calibration both before and after taking Compton scattering data, in order to check for gain shifts.) In this experiment, it was determined that

$$\text{Energy} = 0.1527 \times \text{Channel} - 34.96.$$

Then, using the photopeak values summarized in Table 9.1, we determine the scattered photon energy E' . In Fig. 9.7, we plot the inverse of the measured photon energy, $1/E'$, against $(1 - \cos \theta)$. According to Eq. (9.9), a straight line should be obtained, since

$$\frac{1}{E'} - \frac{1}{E} = \frac{1}{mc^2}(1 - \cos \theta).$$

This is indeed the result, and the slope of the line gives $1/mc^2$ with an intercept at $1/E$. From a least-squares fit we obtain

$$mc^2 = 505 \pm 12 \text{ keV}$$

in very good agreement with the known value of the electron mass. We thus conclude that Eq. (9.9) is very well verified and that our explanation of the Compton frequency shift is firmly supported by these data.

We next turn to the evaluation of the differential cross section. As explained before, we integrate the counts under the photopeak. The results

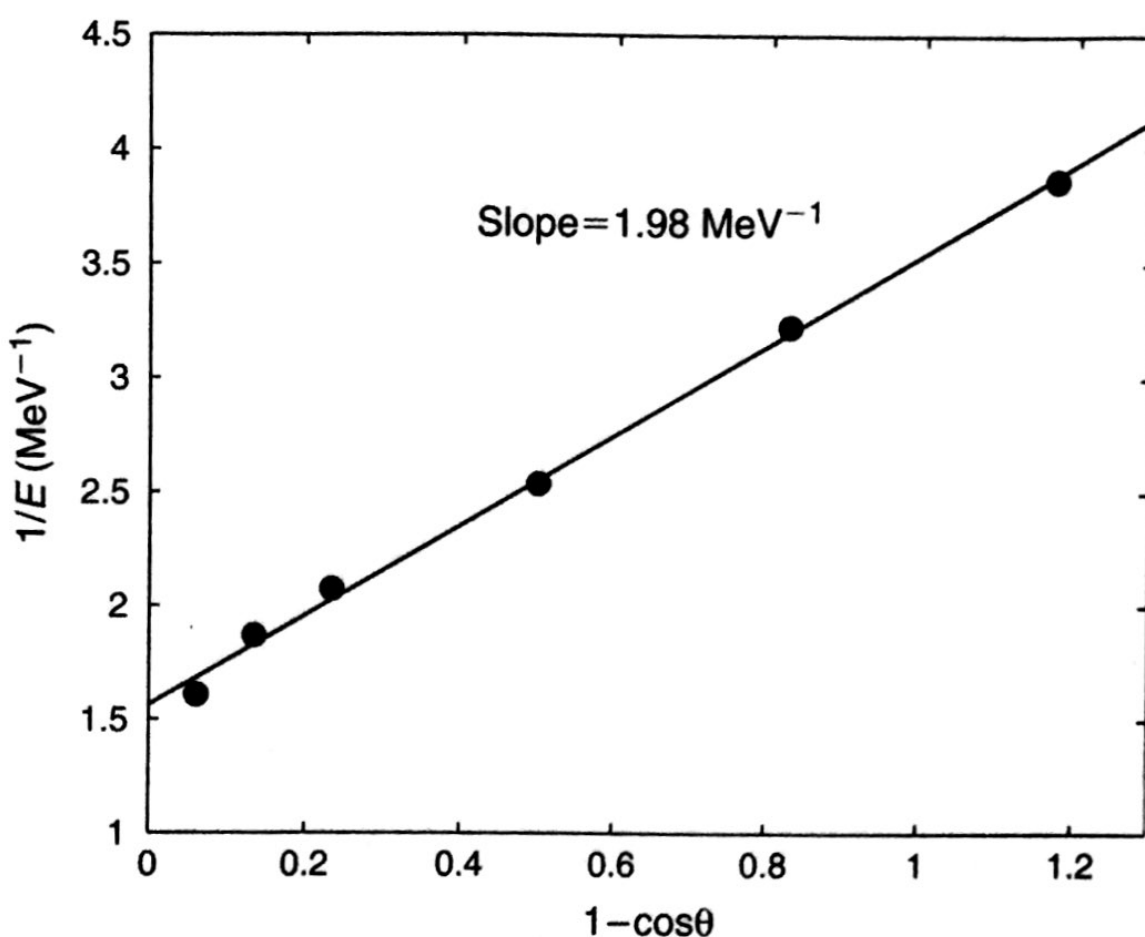


FIGURE 9.7 The results obtained for the energy (frequency shift) of the Compton scattered gamma rays. Note that $1/E$ is plotted against $(1 - \cos\theta)$, leading to a linear dependence. The slope of the line gives the mass of the electron.

are also summarized in Table 9.1. To obtain the cross section we note that

$$\frac{d\sigma}{d\Omega} = \frac{\text{yield}}{(d\Omega)NI_0} = \frac{\text{Total Counts in peak fit}}{\text{Eff. } \omega}$$

The detector solid angle is given by

$$d\Omega = \frac{\text{crystal area}}{r^2} = 6.4 \times 10^{-2} \text{ sr},$$

where r is the distance from the target to the detector. For the total number of electrons in the target, we have

$$N = \pi \left(\frac{d}{2} \right)^2 h \rho \frac{N_0}{A} Z,$$

where⁹

$$d = \text{diameter of target} = \frac{3}{4} \text{ in.} = 1.91 \text{ cm}$$

$$h = \text{height of target} = 4 \text{ cm} \quad \text{Fully within beam}$$

⁹The height of the target is obtained by estimating the length of target intercepted by the beam.

$$\begin{aligned}\rho &= \text{density of aluminum} = 2.7 \text{ gm/cm}^3 \\ N_0 &= \text{Avogadro's number} = 6 \times 10^{23} \\ A &= \text{atomic weight of aluminum} = 27 \\ Z &= \text{atomic number of aluminum} = 13,\end{aligned}$$

thus

$$N = 8.9 \times 10^{24} \text{ electrons.}$$

For I_0 , the flux density at the target, we use the previously obtained value

$$I_0 = 1.3 \times 10^4 \text{ photons/cm}^2\text{-s},$$

and the data acquisition time for each spectrum is 120 s, so that finally

$$\begin{aligned}\frac{d\sigma}{d\Omega} &= \frac{\text{corrected yield}}{(6.4 \times 10^{-2}) \times (8.9 \times 10^{24}) \times (1.3 \times 10^4) \times (120)} \\ &= \frac{\text{corrected yield}}{8.89 \times 10^{29}}.\end{aligned}$$

The values of the differential cross section obtained in this fashion are given in Table 9.1, and are also plotted in Fig. 9.8. The solid line in Fig. 9.8

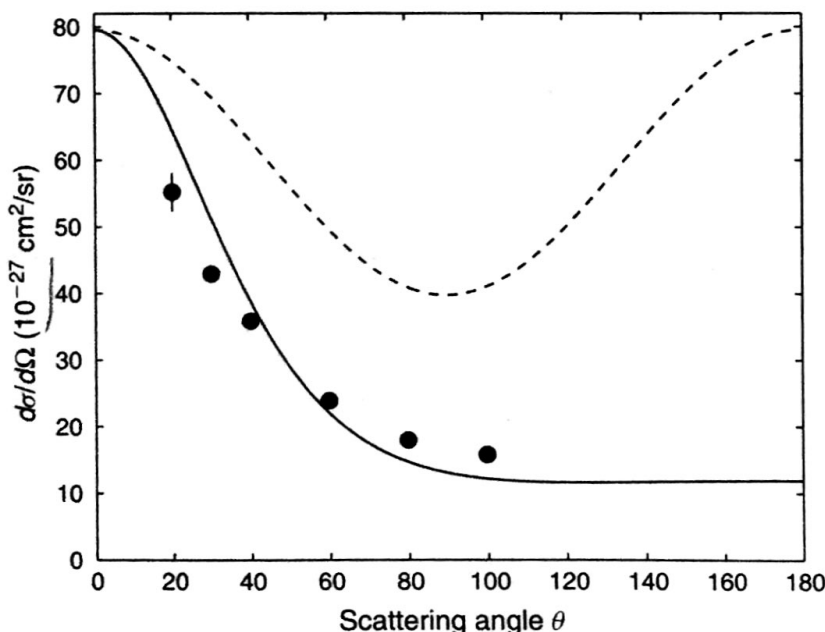


FIGURE 9.8 The results obtained for the scattering cross section of ^{137}Cs gamma rays as a function of angle. The solid line is the prediction of the Klein–Nishina formula for that particular energy; the dotted line is the Thomson cross section.

gives the theoretical values for $d\sigma/d\Omega$ derived from the Klein–Nishina formula (Eq. (9.14)) for $\gamma = 1.29$, while the dashed curve represents the Thomson cross section.

The agreement of the *angular dependence* of the experimental points with the theoretical curve is indeed quite good and clearly indicates the inadequacy of the Thomson cross section for the description of the scattering of high-energy photons, while confirming the Klein–Nishina formula. On the other hand the *absolute value* of the experimental cross section is subject to some uncertainty due to the way in which the flux density I_0 and total number of electrons N were estimated. Nevertheless, the agreement is good.

9.3. MÖSSBAUER EFFECT

9.3.1. General Considerations

In the Compton scattering experiment, we could visualize the scattering process as if it were a collision of two billiard balls in which the incoming photon maintained its identity but suffered a change in momentum and energy. The phenomenon of scattering can, however, also be visualized as the absorption by the target of quanta of the incoming beam, with the subsequent re-emission of these quanta; this was the model we used in the derivation of the Thomson scattering cross section in Section 9.2.

Since we know that emission of quanta of energy $h(\nu_\beta - \nu_\alpha)$ in the visible spectrum is due to transitions of atoms from a state of $\beta \rightarrow \alpha$ we must also expect that when quanta of this energy $h(\nu_\beta - \nu_\alpha)$ are incident on an atomic system in state α , they may be strongly absorbed, with the consequent raising of the atom from state α to state β . Evidence for such strong absorption is obtained by detecting radiation of frequency $(\nu_\beta - \nu_\alpha)$ emitted from the absorber in all directions; it is due to the atoms that, having absorbed a quantum from the beam, were raised to state β and then underwent a spontaneous transition back to state α , emitting the quantum $h(\nu_\beta - \nu_\alpha)$, but with equal probability into all directions. Such radiation is called “resonance radiation” and was first observed by R. W. Wood in sodium vapor in 1904. A schematic of the apparatus is shown in Fig. 9.9. An absorption cell was illuminated by sodium light, and at right angles to the incident beam the sodium *D* lines were observed.